

Shear response behavior of STF/kevlar composite fabric in picture frame test

Yu Ma^{a,b}, Xiang Hong^c, Zhenkun Lei^{c,*}, Ruixiang Bai^c, Yan Liu^c, Jiasheng Yang^d

^a State Key Laboratory of Explosion Science and Technology, Beijing Institute of Technology, Beijing, 100081, China

^b Beijing Institute of Technology Chongqing Innovation Center, Chongqing, 401120, China

^c State Key Laboratory of Structural Analysis for Industrial Equipment, Department of Engineering Mechanics, Dalian University of Technology, Dalian, 116024, China

^d Institute of Fluid Mechanics, Karlsruhe Institute of Technology, Kaiserstraße 12, Karlsruhe, 76131, Germany

ARTICLE INFO

Keywords:

STF/Kevlar composites
Shear thickening fluid
Picture frame test
Shear deformation behavior

ABSTRACT

The picture frame test was applied to compare Kevlar neat and STF/Kevlar composite fabrics. The digital image correlation markers method was applied to measure the shear deformation behavior of the fabric in real-time under three loading rates: 100, 500, and 1000 mm/min. A theoretical model was applied to evaluate the effect of STF on the shear deformation stiffness of the fabric and cells and on the energy absorption during shear deformation. The results show that the STF/Kevlar composite fabric has a larger load-carrying capacity than the neat fabric in the picture frame test, and has obvious loading rate dependence. The yarn cell of the fabric undergoes slip deformation and reaches a shear-locked state; the shear modulus and the cell spring torsion coefficient of the STF/Kevlar composite fabric are significantly higher than those of neat fabric. The shear thickening behavior of STF occurs at higher loading rates, and the composite fabric has the highest shear deformation stiffness and shear energy absorption level.

1. Introduction

Kevlar fiber has good potential for impact protection performance because of the advantages of high strength, high modulus, light weight, and flexibility; thus, it has broad prospects in the field of flexible human protection. The evaluation of impact protection performance of equipment mainly focuses on two aspects: 1) the energy absorption during the impact process and 2) the ability to resist impact deformation [1]. According to the American NIJ protection standard, the depth of the impact basin on the back of the protective equipment in the ballistic interruption test should be less than 44 mm to ensure the safety of protection [2]. For flexible fabrics, although they have the performance advantage of extremely high strength, their soft characteristics rely on large deformation to dissipate the kinetic energy in the process of high-speed impact, which can easily cause non-penetrating damage; therefore, the protection level of flexible human protective equipment is generally lower. The impact process of fabrics includes complex responses such as yarn frictional slippage, shear deformation, and fracture failure [3,4], and a higher shear deformation stiffness will enhance the resistance to impact deformation of a fabric and improve energy absorption during the impact process. Therefore, studying the shear

deformation behavior of fabrics with different shear stiffness has positive significance for the optimal design of the braided impact protection structure and the improvement of the protection level of flexible human protective equipment.

Due to the high-speed transient nature of the fabric penetration process in the ballistic test, the internal behaviors of fabric such as yarn crimping, elongation, frictional slip, shear deformation, and fracture failure are difficult to capture and quantify. Therefore, a series of quasi-static and dynamic modeling test methods are used to quantitatively evaluate the impact response process of fabrics [5–13]. The single-yarn pull-out test is used to quantitatively analyze the interfacial friction behavior of the yarn intersections [5–7], and the off-plane push-out test is used to analyze yarn impact stress distribution behavior [8]. Additionally, the impact basin test is used to quantitatively analyze the impact deformation behavior of the fabric and the impact strain energy level of the yarn [9,10]. Finally, the picture frame and bias extension tests are used for in-depth analysis of the shear deformation and wrinkling behavior of fabrics [11–13].

Bai et al. [5,6] studied the interfacial friction behavior of fabric using the single-yarn pull-out model test method; a bilinear stress transfer model of the yarn interface was established to calculate and analyze the

* Corresponding author.

E-mail address: leizk@dlut.edu.cn (Z. Lei).

frictional energy consumption level of the interface at the intersections during the yarn pulling out process, and the external force response to the yarn pull-out was predicted. Qin et al. [7] conducted Raman spectroscopy measurement and theoretical model analysis on the interface stress transfer behavior of the pulled-yarn intersections during the static friction stage of a single yarn pulling out. The results indicate that, in the process of yarn crimping and elongation, the pull-out load is gradually transmitted at the interface of the intersections along the pulled yarn, and the interface shear stress follows the linear and nonlinear transmission trends in the yarn elongation and crimping regions, respectively. Lei et al. [8] used the off-plane push-out test and Raman spectroscopy to measure the impact stress distribution behavior of three push-out displacements on the fabric. The axial tensile stress of the primary and secondary yarns in 1/4 of the affected surface area were measured by scattered points to calculate the stress distribution of the entire fabric surface. The results showed that the stress level of the primary yarn is significantly higher than that of the secondary yarn, and the surface stress of the fabric presents a cross shape distribution state. Additionally, with an increase in the push-out displacement, the stress difference between the primary yarn and the secondary yarn also gradually increases. Ma et al. [9,10] carried out the impact basin test to analyze the impact deformation mechanism of the fabric and impact strain energy of the yarn. A method for evaluating the impact protection performance of fabrics based on the 3D morphology of impact basins was proposed, and the impact deformation attenuation function of impact basins was determined to quantitatively evaluate the transmission efficiency of impact stress waves between yarns.

The picture frame test can intuitively evaluate the shear deformation behavior of knitted fabrics [11–13]. Compared with several other test methods (especially the single-yarn pull-out test), the picture frame test is obviously underestimated. Only a few related works have been published, and they have focused on the shear deformation process of fabric compression molding. Harrison et al. [11] proposed a normalization procedure for the uniaxial bias extension test to directly compare the picture frame test results, determine the shear-lock angle, and compensate for the adverse effects of boundary conditions in the picture frame test. Nosrat et al. [12] conducted a novel picture frame shear test on the shear deformation behavior of plain weave fabrics in both relaxed and tensioned states. The results showed that there is a nonlinear relationship between the global deformation response and the initial pre-load of the flexible fabric. Moezzi et al. [13] conducted an experimental study on the shear deformation and wrinkling behavior of UV-exposure-aged fabrics through the uniaxial bias extension test and image processing; they clarified the effect of local uneven aging caused by UV exposure on the shear deformation process.

Shear thickening fluid (STF) is a non-Newtonian fluid, usually a colloidal suspension prepared by mixing dispersed phase powder and dispersant solution through physical stirring, and the material properties are sensitive to the external stress environment. STF exhibits good fluidity in a static environment, but when subjected to impact loads, the interior will undergo a micro-cluster phase change within microseconds, making the macroscopic properties similar to a solid state, and significantly improving the energy absorption [14,15]. Therefore, composite fabrics reinforced by STF impregnation typically have better impact protection and have become a research hotspot in related fields [16,17]. Cao et al. [16] and Xu et al. [17] used high-modulus material multi-walled carbon nanotubes and high-hardness material B₄C particles to strengthen single-phase STF, which was then used to prepare multi-phase STF materials. Subsequently, a “dipping-drying” process was used to prepare multi-phase STF/Kevlar composite fabric, and finally, the single yarn pull-out and ballistic penetration tests were conducted. The results showed that multi-phase STF/Kevlar composite fabrics have a higher level of interfacial friction compared with that of neat fabric, and its ballistic limit and energy absorption are also significantly improved.

In this study, industrial SiO₂ with an average particle size of 1 μm

was used as the dispersed phase, and ethylene glycol (EG) was used as the dispersant. STF with a mass fraction of 70% was prepared by the planetary ball milling method, and the STF rheological analysis was performed. STF/Kevlar composite fabrics were further prepared by applying STF using the “dipping-drying” process on Kevlar plain fabrics. Picture frame tests were carried out on neat and STF/Kevlar composite fabrics under three loading rates, and the displacement of markers on the fabric surface was measured in real time with the digital image correlation (DIC) method. The shear deformation behavior was quantitatively evaluated, the spring torsion coefficient of the woven cells of neat and STF/Kevlar composite fabrics was calculated, and the shear deformation stiffness and energy absorption of the fabrics were output. Finally, the enhancement of STF on the shear deformation behavior of the fabric is evaluated.

2. Experimental setup

2.1. Material properties

In this study, Kevlar 49 plain fabric (DuPont) was used to study the shear behavior. The basic parameters are listed in Table 1, and the weaving geometry is shown in Fig. 1.

Plain fabric is made of vertical warp yarns and horizontal weft yarns. Both warp and weft yarns are composed of a large number of fiber filaments (Fig. 1(a)). The number of fiber filaments in each bundle is 1000 pieces (Table 1). The weaving trajectories of the warp and weft are shown in Fig. 1(b) and (c), respectively. The warp and weft are woven in contact with each other through numerous intersections, and there is a slight difference between the weaving geometric parameters [6], which was not considered in this study.

The warp and weft weaving trajectories are shown in Fig. 1(d) and (e), respectively. The warp has a larger crimp trajectory and a more “wide and thin” cross-section relative to the weft. Conversely, the weft has a smaller crimp trajectory but a more “narrow and thick” cross-section, which is due to the different weaving force that the weaving machine exerts on the warp and weft yarns. W_a and W_b represent the widths, T_a and T_b represent the thicknesses, and G_a and G_b represent the gaps of weft and warp, respectively. For simplicity of calculation, the difference in warp and weft yarn size is ignored, and the average value is used instead. Here, the equivalent width W is the average value of the width of the warp and weft intersections when considering the gap; the equivalent thickness T is the average thickness of the warp and weft yarns, as listed in Table 2.

The cross-sectional area of the yarn (A_c) can be calculated as

$$A_c = N\pi D_f^2 / 4 \quad (1)$$

where D_f is the fiber diameter, and N is the number of single fibers in a single yarn. Based on the data in Tables 1 and 2, the cross-sectional area is $A_c \approx 0.113 \text{ mm}^2$.

2.2. Shear thickening fluid

Using SiO₂ powder with an average particle size of 1 μm (Fucai Mineral Material Products Co., Ltd.) as the dispersed phase and EG (Sinopharm Chemical Reagent Co., Ltd.) as the dispersant to configure the STF, the process was prepared, as shown in Fig. 2.

First, large amounts of organic matter and inorganic salt impurities

Table 1
Basic parameters of Kevlar 49 plain fabric.

Material	Linear density (Dtex)	Areal density (g/m ²)	Number of fibers, N	Fiber diameter D_f (μm)
Kevlar 49	1580	240	1000	12

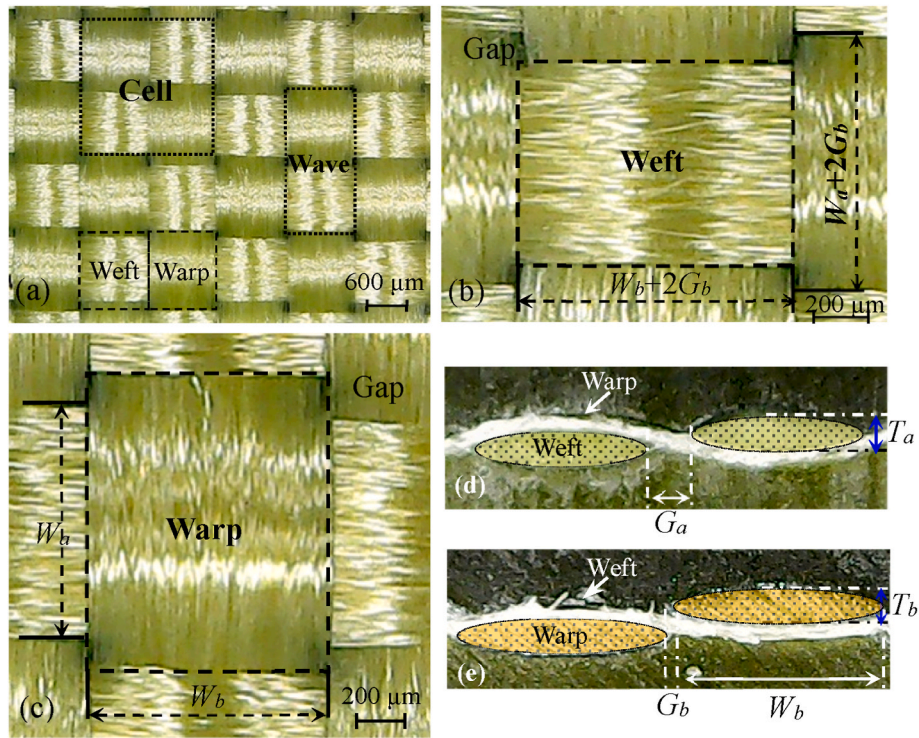


Fig. 1. Schematic of Kevlar 49 plain fabric; (a–c) braided geometry structure; (d) warp trajectory; (e) weft trajectory.

Table 2
Geometric dimensions of Kevlar 49 plain fabric (Unit: mm).

Yarn	Width	Gap	Equivalent width	Thickness
Weft	$W_a = 1.0$	$G_a = 0.1$	$W_a + 2G_a = 1.2$	$T_a = 0.23$
Warp	$W_b = 1.1$	$G_b = 0.05$	$W_a + 2G_a = 1.2$	$T_b = 0.24$
Average value	/	/	$W = 1.2$	$T = 0.235$

are doped in industrial SiO₂ particles, which could affect the performance of STF materials to a certain extent, so it was necessary to wash and purify the SiO₂ dispersed phase. In the washing process, deionized water and absolute ethanol were used for cleaning with an ultrasonic water bath oscillation for 20 min. After the oscillation was completed, centrifugation was performed to precipitate SiO₂ particles on the bottom of the bottle to clear the surface impurities. The deionized water and absolute ethanol washing process was performed three times, and then the drying and grinding processes were carried out to obtain a neat SiO₂

dispersed phase, as shown in Fig. 2(a). In the second step, the purified SiO₂ dispersed phase and EG dispersant (Fig. 2(b)) were mixed and configured according to the mass fraction of 70 wt.% and placed in a ball mill (Fig. 2(c)) for grinding. After stirring for 24 h, the STF preparation was complete (Fig. 2(d)). Finally, the rheological properties of the prepared STF were measured with an Anton Paar MCR301 rheometer (Fig. 2(e)). The results show that, as the shear rate gradually increased from 1 s⁻¹ to 300 s⁻¹, the STF viscosity curve experienced first a slight decrease and then a significant increase. The STF viscosity gradually decreased from 9 Pa·s to 1.5 Pa·s in the shear rate range of 1–18 s⁻¹, and this stage is defined as shear thinning. As the shear rate continued to increase beyond 18 s⁻¹, the STF viscosity increased significantly and reached the limiting viscosity level of 400 Pa·s at a shear rate of 62 s⁻¹, defined as shear thickening; the shear rate of 18 s⁻¹ is the “threshold” for shear thickening behavior to occur.

The STF/Kevlar composite fabric was prepared by the “dipping-drying” method. First, the STF was diluted with absolute ethanol (mass

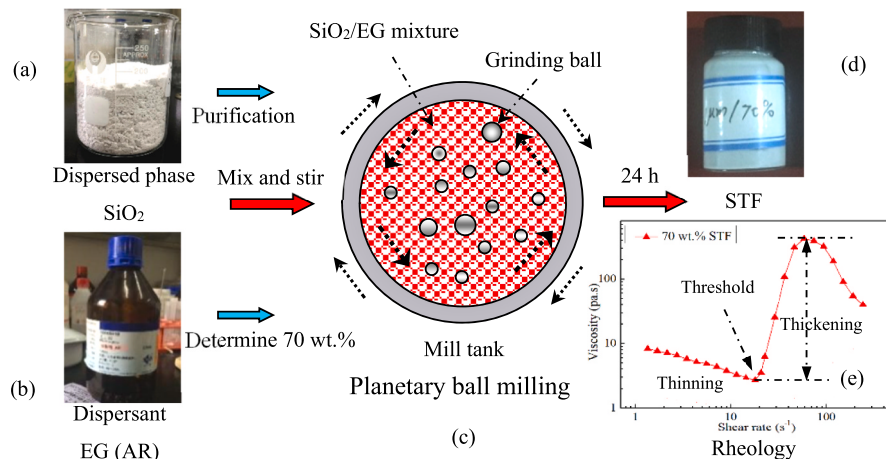


Fig. 2. STF preparation process and rheological properties curve [10].

ratio 1:2), and the Kevlar fabric was soaked in the mixed solution and subjected to ultrasonic water bath oscillation for 20 min to increase the degree of impregnation. After the impregnation was completed, the Kevlar fabric was taken out and dried at 50 °C and weighed every 2 min. When the results of two consecutive weightings did not change, the absolute ethanol was considered completely volatilized, and the STF/Kevlar composite fabric was completely prepared. The STF surface attachment state on the Kevlar fabric was characterized by scanning electron microscopy (SEM), as shown in Fig. 3.

For the neat fabrics (Fig. 3(a) and (b)), the overall surface is in a relatively smooth state, with only a small amount of dust and filamentous impurities attached. This is related to the storage environment of the flexible fabric, and the natural impurities on these surfaces do not significantly affect the interfacial properties of flexible fabrics [18]; therefore, they are not considered in this study.

For the STF/Kevlar composite fabrics (Fig. 3(c) and (d)), a large amount of STF is adhered to the surface of the fabric, which significantly increases the roughness of the yarn surface, thereby improving the friction performance of the yarn interface. Moreover, STF has largely filled in the gaps between the Kevlar filaments, and its high viscosity properties significantly enhance the connection between filaments and yarns, which will limit the mutual sliding behavior of yarns when the fabric is deformed [5,6].

2.3. Picture frame test

In this study, the picture frame test was used as a quasi-static modeling method for the ballistic penetration process of flexible fabrics to quantitatively evaluate the effect of the shear deformation behavior of flexible fabrics on the impact protection performance. The picture frame test was applied to Kevlar 49 plain fabric and STF/Kevlar composite fabric, and the experimental setup is shown in Fig. 4(a), where the middle square area is the effective area of shear deformation, and its side length is $L = 180$ mm. The displacement loading method was adopted, and the influence of the loading rate on the shear deformation behavior of the fabric was considered with three preset loading rates of

100, 500, and 1000 mm/min. In the deformation effective area, the fabric surface was calibrated by a markers matrix and combined with the DIC method to measure the shear deformation state. Due to the symmetry of the overall deformation of the fabric during the test, to reduce repeated data and workload, the deformation measurement was only performed on 1/4 of the specimen, as shown in Fig. 4(b).

The markers matrix is based on the boundary of the shear deformation effective area of the fabric specimens, and the distance between the rows and columns of the markers is 15 mm; thus, the connecting distance between markers 1 and 7 in Fig. 4(b) is 90 mm. The boundary angle is $\theta = 45^\circ$ in the initial state of the fabric specimen before loading. The fabric specimen undergoes shear deformation during the loading process, the displacement state of the surface marker matrix is output, and with the tensile load, the shear deformation behavior of the fabric specimen can be quantitatively analyzed.

During the picture frame test of the fabric, the load curve is divided into two stages, and the slopes are obviously different. The bilinear external load is caused by the shear-locking behavior of the fabric. After the shear-locking behavior occurs, the inner yarn is tightly compacted, the load-bearing capacity is significantly improved, and wrinkles appear on the surface of the fabric after further loading [19]. The shear-locking behavior is more obvious in the process of fabric compression molding, but the impact force is concentrated on the primary yarn during the fabric impact process, and fabrics tend not to achieve the shear-locking state. However, the shear deformation behavior significantly affects the kinetic energy transfer efficiency of the bullet between yarns. Therefore, this study focuses on the mechanical response characteristics of the fabric before shear-locking behavior occurs.

3. Results and discussion

3.1. Load-displacement curve

Fig. 5 shows the load-displacement curves of the picture frame shear test for neat and STF/Kevlar composite fabrics at three loading rates.

It can be seen from Fig. 5 that the neat and STF/Kevlar composite

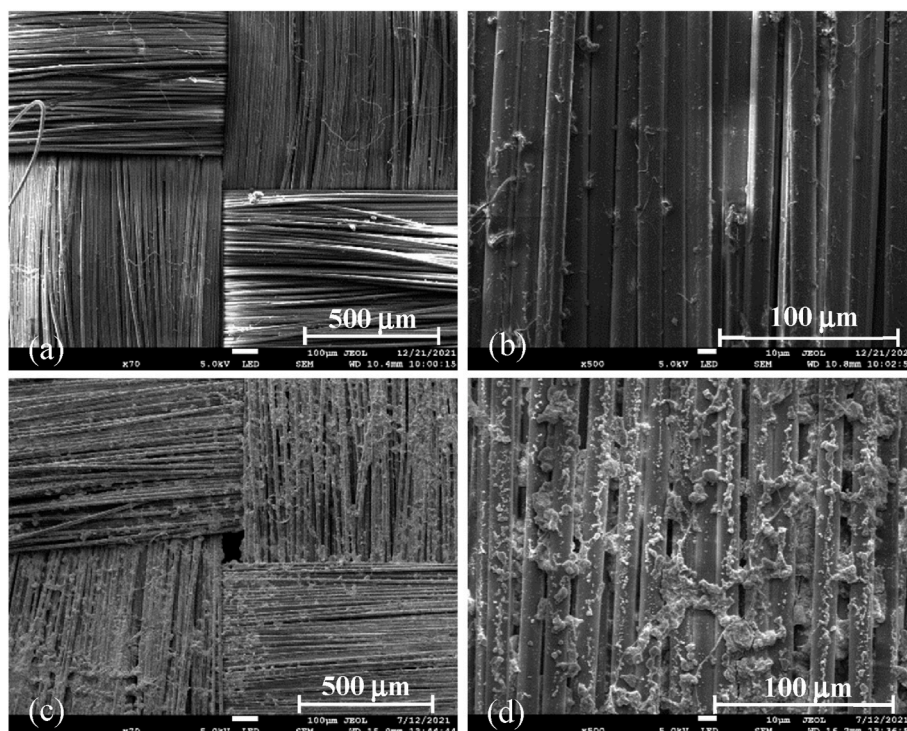


Fig. 3. STF/Kevlar composite fabric surface with scanning electron microscope; (a), (b) neat fabric; (c), (d) STF/Kevlar composite fabric.

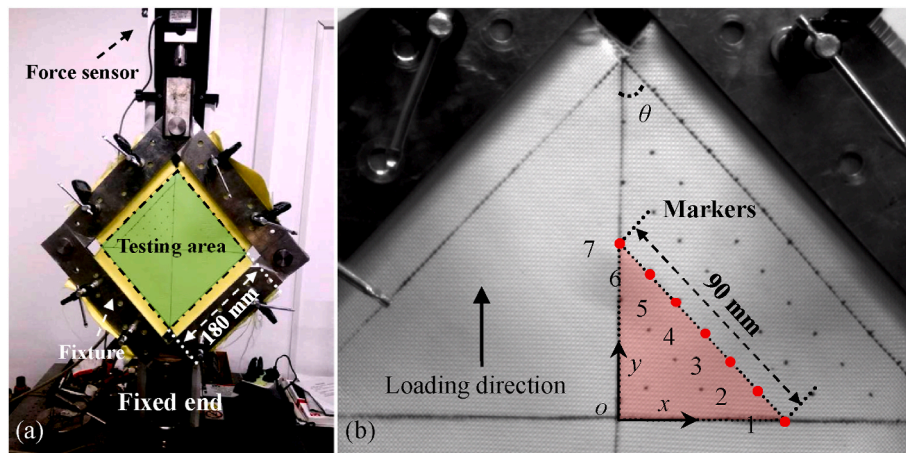


Fig. 4. Photo frame test; (a) experimental setup; (b) markers matrix.

fabric specimens both achieve shear locking when the loading displacement reaches approximately 60 mm and then stops loading. For the neat fabrics, the load-displacement curves show a linear upward trend at the three loading rates and are not significantly affected by the loading rate. When the fabric reaches a shear-locking state, the external load is approximately 400 N (Fig. 5(a)). For the STF/Kevlar composite fabrics, the load-displacement curves show a nonlinear upward trend at the three loading rates, and there is an obvious correlation with the loading rate. The STF/Kevlar composite fabrics have the highest load-carrying capacity at a 1000 mm/min loading rate, with an external load of approximately 750 N in the shear-locked state; the lowest load-carrying capacity is at a 500 mm/min loading rate, with an external load of only 450 N in the shear-locked state; at a loading rate of 100 mm/min, the external load of the composite fabric is approximately 600 N in the shear-locked state. The correlation between the load-carrying capacity and loading rate of STF/Kevlar composite fabrics is considered to be the effect of STF shear thinning and shear thickening behavior.

3.2. Shear deformation

The shear deformation states of the fabric during the picture frame test are shown in Fig. 6(a), (b), and (c), corresponding to the initial state before loading, the deformation process, and the maximum deformation state, respectively. To ensure that the fabric shear deformation state was not affected by the boundary conditions of the picture frame fixture, the DIC method only measured the deformation state of the red triangle area in Fig. 6(a).

It can be seen from Fig. 6(a) that the length of the hypotenuse of the measured triangle area is 90 mm and the upper angle is $\theta = 45^\circ$;

therefore, the distance between the #7 marker and the coordinate origin can be calculated using the Pythagorean theorem as approximately 63.6 mm. The displacements of markers #1 ~ #7 (Fig. 4(b)) in the y-direction of the fabric specimens at a 100 mm/min loading rate were calculated and output to evaluate the shear deformation state of the fabric, as shown in Fig. 7. The 500 and 1000 mm/min loading rate results are listed in the Appendix.

It can be seen from Fig. 7 that both the neat and STF/Kevlar composite fabrics are in a shear-locking state at approximately 37.5 s at a loading rate of 100 mm/min, and the displacement of the markers are no longer rising and then stops loading. The maximum displacement (11.1 mm) of marker #7 on the surface of the neat fabric is slightly smaller than that of the STF/Kevlar composite fabric (12.8 mm), but the maximum shear load (603 N) of the STF/Kevlar composite fabric is significantly higher than that of the neat fabric (396 N), as shown in Fig. 5.

According to the displacement of the markers on the fabric surface during the shear deformation process, the angle θ of the triangular area in Fig. 6(b) and (c) can be calculated and output to obtain the shear angle 2θ of the fabric specimen, as shown in Fig. 8(a). Then, the shear strain of the fabric specimen is analyzed, as shown in Fig. 8(b).

It can be seen from Fig. 8(a) that under the shear load, the shear angle of the neat and STF/Kevlar composite fabrics gradually decreases, and there is a linear downward trend overall until the shear-locking state is reached. The black dotted line in the figure corresponds to the load of the neat fabric in the locked state, and the red dotted lines correspond to the loads of the STF/Kevlar composite fabric when it reaches the locked state for three different loading rates. The locking load of the STF/Kevlar composite fabric is significantly higher than that of the neat fabric, and

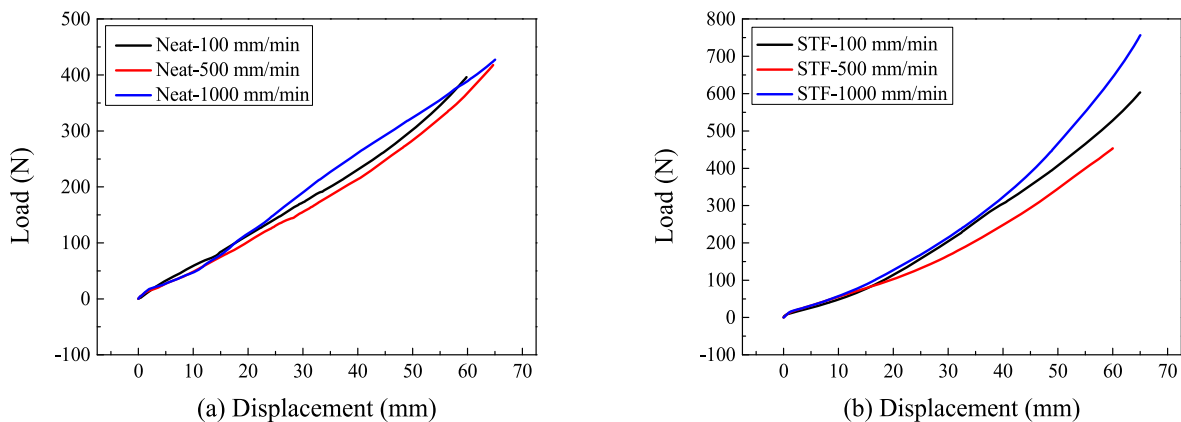


Fig. 5. Load-displacement curves for (a) neat and (b) STF-Kevlar fabric at three loading rates.

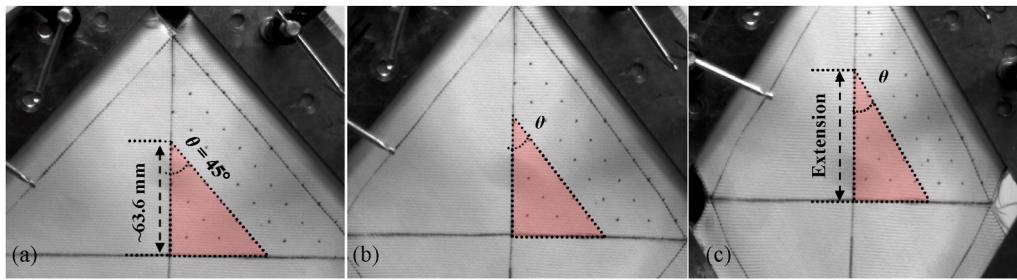


Fig. 6. (a) Initial state, (b) deformation process, and (c) maximum deformation for fabric under shear deformation.

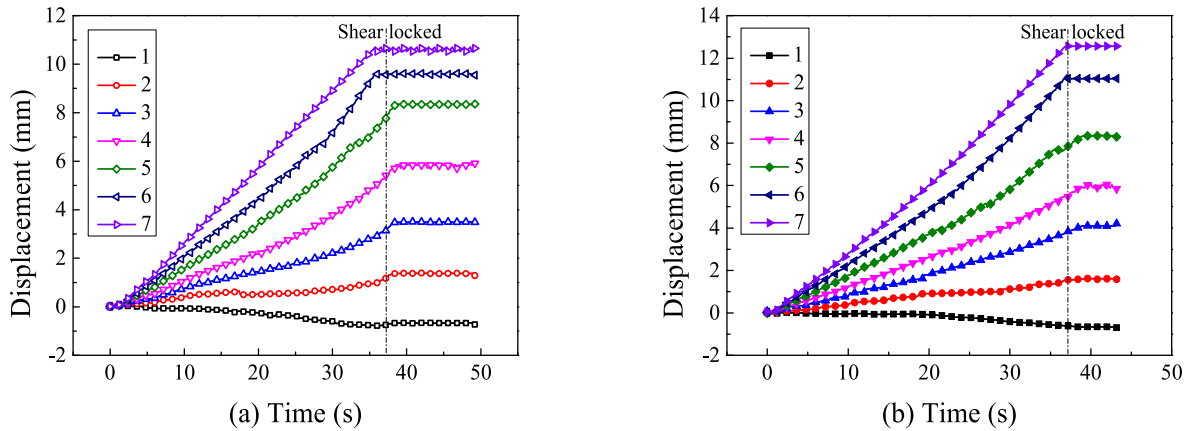


Fig. 7. Displacement in y-direction of #1 ~ #7 markers for (a) neat fabric and (b) STF/Kevlar composite fabric at 100 mm/min loading rate.

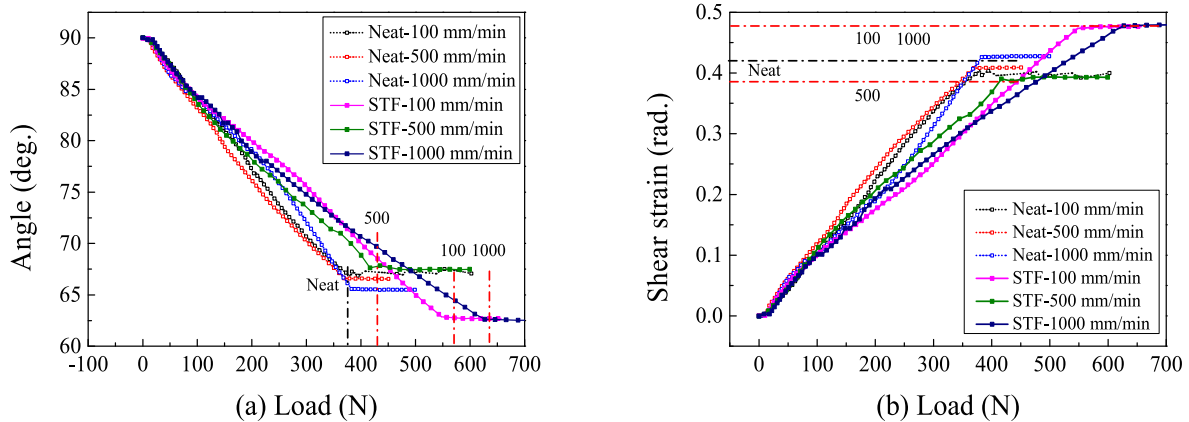


Fig. 8. Curves of (a) shear angle and (b) shear strain vs. load of neat and STF/Kevlar composite fabrics at three loading rates.

the locking load of the composite fabric under different loading rates is significantly different. The locking load at a 500 mm/min loading rate is the lowest (420 N), which corresponds to the STF shear thinning behavior; the locking load at 1000 mm/min loading rate is the highest (630 N), which corresponds to STF shear thickening behavior.

It can be seen from Fig. 8(b) that the shear strain variation trend of neat and STF/Kevlar composite fabrics is similar to that of shear angle: with the gradual increase of shear load, the shear strain of the fabric specimen shows a linear upward trend. The black dotted line corresponds to the locked shear strain of neat fabric, and the red dotted lines correspond to the locked shear strain of STF/Kevlar composite fabric. The variation range of fabric shear angle θ and shear strain γ of neat and STF/Kevlar composite fabrics at three loading rates are listed in Table 3.

It can be seen from Table 3 that the shear-locking angle and shear strain of the neat fabric did not change significantly at the three loading

rates, indicating that the shear deformation mechanism of the neat fabric was not affected by the loading rate. In contrast, the shear angle and shear strain of the STF/Kevlar composite fabric were different at the three loading rates, and this difference was considered to be the shear mechanism difference of the composite fabrics caused by the shear

Table 3

Variation range of shear angle θ and shear strain γ of neat and STF/Kevlar composite fabrics at three loading rates.

Specimen	Variation	100 mm/min	500 mm/min	1000 mm/min
Neat	Shear angle θ ($^{\circ}$)	[45, 33.55]	[45, 33.26]	[45, 32.91]
	Shear strain γ (rad)	[0, 0.399]	[0, 0.410]	[0, 0.422]
STF/Kevlar	Shear angle θ ($^{\circ}$)	[45, 31.31]	[45, 33.64]	[45, 31.24]
	Shear strain γ (rad)	[0, 0.478]	[0, 0.396]	[0, 0.480]

thinning and shear thickening behaviors of STF.

Under the action of shear force, the inner yarn of the neat and STF/Kevlar composite fabrics gradually slipped and reached shear locking after the initial, slip, and extrusion stages, as shown in Fig. 9.

In the initial stage before the fabric is subjected to shear load (Fig. 9 (a)), the entire braided structure is in a loose state, and there is a large gap between adjacent warp and weft yarns. When the fabric is subjected to shear load, the warp and weft yarns slip with each other, the yarn gap and shear angle θ begin to decrease, and the fabric exhibits overall shear deformation (Fig. 9(b), the slip stage). As the shear deformation continues to increase, the yarn gap decreases, contact between adjacent warp and weft yarns occurs, and contact stress is generated (Fig. 9(c), the extrusion stage). At this point, the fabric begins to shear lock (corresponding to the locking angle), and with the continued application of an external load, the load-displacement curve shows an obvious nonlinear trend, and wrinkles appear on the surface of the fabric [11, 13]. In this study, only the fabric shearing behavior before the fabric shear-locking stage is studied and discussed.

Because the surface of neat fabric yarn is relatively smooth (Fig. 3(a) and (b)), under the action of shear force, it will rapidly slip and reach the extrusion stage, resulting in shear locking. The large amount of STF attached to the yarn surface of the STF/Kevlar composite fabric fills in fiber gap. In the process of shear deformation, the damping effect of STF will limit the yarn slip [5,6] and allow the fabric specimen to carry a larger load; meanwhile, the in-plane shear load of the fabric is more uniform. Therefore, in the process of shear deformation, the state of the yarn is gradually adjusted. The larger external load also produces a larger contact stress between the yarns, making the yarn more compact; thus, the overall shear deformation of the STF/Kevlar composite fabric is slightly larger than that of the neat fabric.

3.3. Shear modulus

In the picture frame test, there is a corresponding geometric relationship between the external load P and the shear force F_s of the fabric specimen, as shown in Fig. 10.

From Fig. 10, the relationship between the external load P and the shear force F_s can be given as

$$P = 2F_s \cos \theta \quad (2)$$

where F_s is the shear force that the load P resolves in the direction of the frame. Then, the shear stress τ can be obtained from the shear force F_s and the cross-sectional area S of the fabric, namely

$$\tau = \frac{F_s}{S} = \frac{F_s}{nA_c} = \frac{WF_s}{LA_c} \quad (3)$$

Here, A_c is the cross-sectional area of a single yarn, which is calculated by Eq. (1). n is the number of intersections of warp and weft yarns and can be obtained by converting the side length L of the fabric and the equivalent width W of the yarn in Table 2 ($n = L/W$). It can be seen from Fig. 1(d) and (e) that the cross-section of the fabric is composed of

several elliptical cross-sections of yarns, and the cross-sectional area S can be obtained by summing the cross-sectional areas of all warp and weft yarns, that is, $S = nA_c$.

For the Kevlar 49 plain fabric, the yarn cross-sectional area $A = 0.113 \text{ mm}^2$. In addition, from the equivalent width W of the yarn (Table 2), the cross-section of the fabric specimen is approximately $n = 150$ elliptical cross-sections of the yarn, with $S = 16.95 \text{ mm}^2$. Therefore, according to Eq. (3), the shear stress τ of the fabric, the shear strain of the fabric measured by the DIC markers method (Fig. 8(b)), and finally, the shear stress-strain curve of neat and STF/Kevlar composite fabrics at three loading rates are obtained, as shown in Fig. 11(a).

The shear stress-strain curves of the neat and STF/Kevlar composite fabrics in the picture frame test are linear at the three loading rates, and a linear fit is performed on the shear stress-strain curves in Fig. 11(a) to resolve the slopes of the curves more clearly, as shown in Fig. 11(b). For the neat fabric, the shear modulus is independent of the loading rate; in contrast, the shear modulus of the STF/Kevlar composite fabric is related to the loading rate, and the highest shear modulus is at the loading rate of 1000 mm/min. According to the slopes of the shear stress-strain curves in Fig. 11(b), the shear moduli of the neat and STF/Kevlar composite fabrics at three loading rates are output, as shown in Fig. 12 (a).

The areas below each displacement loading step of the load-displacement curves (Fig. 5) in the picture frame test were integrated and calculated to obtain the energy absorption curves of the fabrics, as shown in Fig. 12(b).

There is only a small difference (31–33 MPa) in the shear moduli of the neat fabrics at three loading rates, indicating that the shear deformation stiffness of the neat fabrics is not significantly related to the loading rate. In contrast, the shear modulus of the STF/Kevlar composite fabric is at the minimum (38 MPa) at a loading rate of 500 mm/min (still significantly higher than that of the pure fabric), corresponding to the shear thinning behavior of STF at a loading rate of 500 mm/min, and the maximum is 48 MPa at 1000 mm/min, corresponding to the shear thickening behavior of STF.

The STF/Kevlar composite fabric has larger energy absorption than the neat fabric during the shear deformation process, and it is obviously related to the loading rate. At the rate of shear thickening of STF, the maximum energy absorption of the composite fabric can reach 18.5 J. In contrast, the energy absorption of neat fabric has only a small change in the shear deformation process under the three loading rates. Compared to the overall energy absorption of the fabric, the difference in energy absorption can be caused by the different fabric boundary clamping preload conditions.

3.4. Theoretical model

From Fig. 10(b), the shear strain γ of the fabric during the picture frame test can be expressed as

$$\gamma = (90^\circ - 2\theta) \frac{\pi}{180} \quad (4)$$

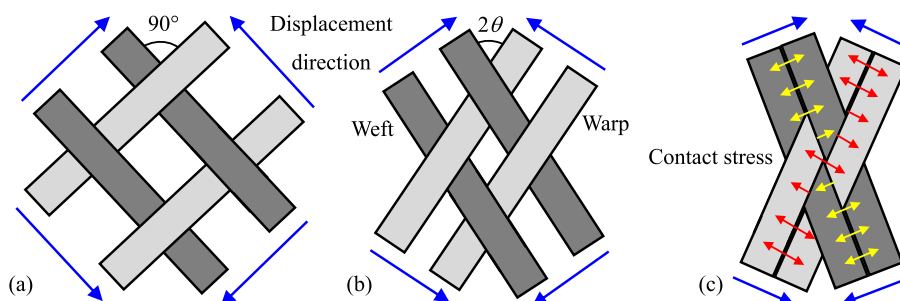


Fig. 9. (a) Initial stage, (b) slip stage, and (c) extrusion stage for fabric shear deformation.

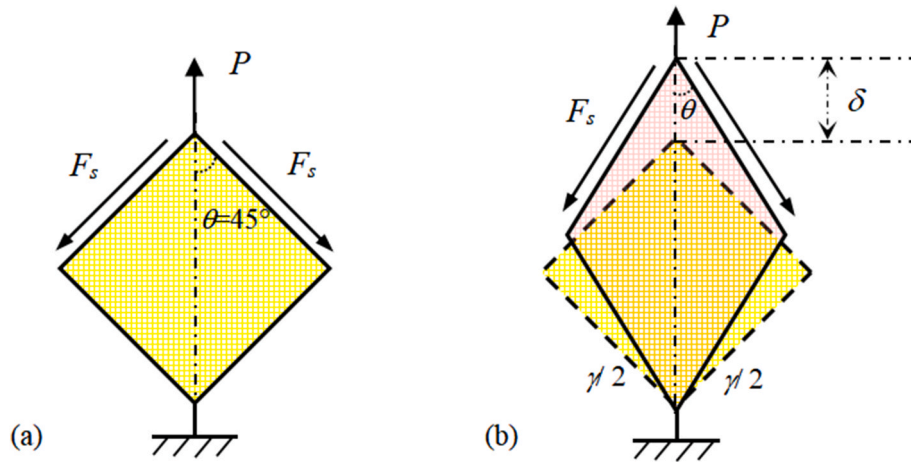


Fig. 10. Force analysis of the fabric under tension shearing; (a) before loading; (b) after loading.

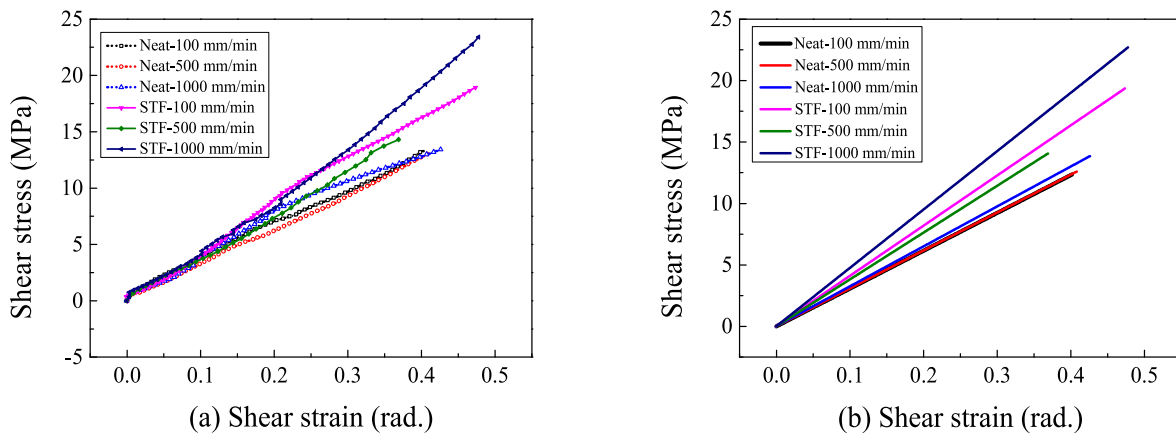


Fig. 11. (a) Shear stress-strain curves and (b) linearly fitted results for neat and STF/Kevlar composite fabrics at three loading rates.

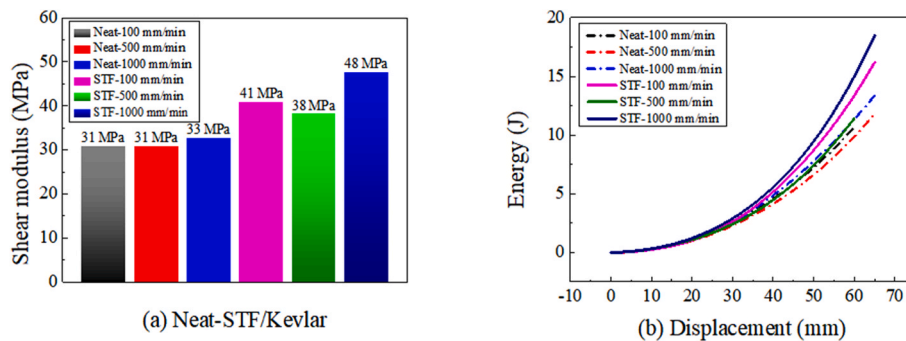


Fig. 12. (a) Shear moduli and (b) energy absorption curves for neat and STF/Kevlar composite fabrics at three loading rates.

where θ is the shear angle of the fabric (Fig. 4(b)). Then, the diagonal length D of the fabric specimen after shear deformation can be expressed as

$$D = \sqrt{[(L \cos \gamma)^2 + (L \sin \gamma + L)^2]} = L\sqrt{2 + 2 \sin \gamma} \quad (5)$$

Here, L is the side length of the fabric specimen (Fig. 4(a)). When the shear strain is zero, i.e., $\gamma = 0$, the above Eq. (5) degenerates into the original diagonal length of the fabric specimen. According to the geometry, the relationship between shear strain γ and load displacement δ is obtained as

$$\delta = L\sqrt{2 + 2 \sin \gamma} - L\sqrt{2} \quad (6)$$

Before shear locking occurs, the fabric mainly resists the external force through the rotational friction between the yarns; thus, for a weaving cell (Fig. 1(a)), the rotational friction between the yarns during the shear deformation process can be characterized by two torsion springs on the diagonal, and the force states are shown in Fig. 13.

The shear deformation behavior of fabric can be characterized by the process of the internal weaving cells slipping and gradually converging [20]. There are torsion springs on both diagonals of the cell to generate a force F in the opposite direction (Fig. 13), which has a linear relationship

with the torsion angle γ , that is,

$$F = k\gamma \quad (7)$$

where k is the spring torsion coefficient. For simplification, when the rotation strain γ is generated, the torque generated by the torsion force F on the center of the cell is considered to be perpendicular to the diagonal of the quadrilateral cell; thus, the torque generated by the torsion force F at approximately the center point o of the cell is

$$M_F = Fd \quad (8)$$

Here, d is the diagonal length of the cell, which can be derived according to Eq. (5), namely

$$d = l\sqrt{2 + 2\sin\gamma} = 2W\sqrt{2 + 2\sin\gamma} \quad (9)$$

where the cell side length $l = 2W$. Combining Eqs. (1) and (9), Eq. (8) can be rewritten as

$$M_F = 2Wk\gamma\sqrt{2 + 2\sin\gamma} \quad (10)$$

Further, assuming that the shear force is uniformly borne by all cells, the shear force carried by each cell can be expressed as

$$f_s = \frac{F_s}{n_c} = \frac{F_s}{L}l = \frac{2WF_s}{L} \quad (11)$$

where $n_c = L/l = n/2$ is the number of weaving cells, which is equal to half of the warp and weft intersections. Then, the moment of the shear force f_s to the cell center can be expressed as

$$M_f = f_s l \cos\gamma = \frac{4F_s W^2}{L} \cos\gamma \quad (12)$$

From the moment balance condition $M_F = M_f$, the relationship between the shear force F_s and the shear deformation γ of the fabric in the picture frame test can be obtained as

$$F_s = \frac{Lk\gamma\sqrt{2 + 2\sin\gamma}}{2W \cos\gamma} \quad (13)$$

Further, combining Eqs. (3) and (13), the constitutive relationship between shear stress and shear strain is obtained as

$$\tau = \frac{k\gamma\sqrt{2 + 2\sin\gamma}}{2A_c \cos\gamma} \quad (14)$$

Under the assumption of small deformation, with $\sin\gamma \approx \gamma$ and $\cos\gamma \approx 1$, Eq. (14) can be simplified to

$$\tau \approx \frac{k\gamma\sqrt{2 + 2\gamma}}{2A_c} \approx \frac{k}{A_c}\gamma = G\gamma \quad (15)$$

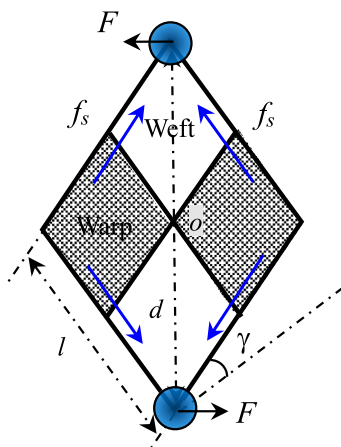


Fig. 13. Schematic of shear force state of a weaving cell.

where G is the shear modulus. Under the assumption of small deformation, the shear stress and shear strain have an approximate linear relationship, consistent with the trend of the shear stress-shear strain experimental curve (Fig. 11(b)).

Combined with the fitting data of shear stress and shear strain (Fig. 11(b)), the cell spring torsion coefficient k can be calculated according to Eq. (14), and the shear deformation stiffness of the yarn weaving cell can be quantitatively evaluated. The cell spring torsion coefficients of the neat and STF/Kevlar composite fabrics at three loading rates were calculated and are listed in Table 4.

It can be seen from Table 4 that the cell spring torsion coefficient of STF/Kevlar composite fabric is larger than that of the neat fabric as a whole, indicating a higher shear deformation stiffness and the same trend as the shear moduli of the fabric specimens (Fig. 12 (a)). The variation range of the torsion coefficient of the neat fabric weaving cell spring under the three loading rates is small, only 0.25 N/rad. However, there is a clear relationship between the viscosity of STF and the loading rate, and it is directly reflected in the spring torsion coefficient k of the weaving cell. Under the loading rate of 500 mm/min, the STF has a shear thinning effect and a slight drop in viscosity level relative to the 100 mm/min loading rate; the corresponding restriction on yarn slip decreased, and the cell spring torsion coefficient k decreased slightly. At the loading rate of 1000 mm/min, the shear thickening effect of STF occurs, the viscosity level increases significantly, the relative slippage restriction between the yarns is enhanced, and the weaving cell has the highest level of spring torsion coefficient k , which reached 6.18 N/rad.

Moreover, under the assumption of small deformation, combined with the experimental data of the shear modulus G (Fig. 12(a)), the cell spring torsion coefficient $k \approx GA_c$ can be calculated according to Eq. (15). For example, the shear modulus of STF/Kevlar composite fabric is 48 MPa at the loading rate of 1000 mm/min, and the torsion coefficient of the cell spring is $k = 5.42$ N/rad, which is only slightly lower than the corresponding data in Table 4 (6.18 N/rad). Therefore, the small deformation assumption is appropriate for the friction stage of fabric in the picture frame shear test.

4. Conclusion

In the picture frame test, the mechanical response of neat and STF/Kevlar composite fabrics showed a significant difference. The load-displacement curve of the neat fabric showed a linear distribution overall, and there was no obvious correlation with the loading rate. In contrast, the load-displacement curve of the STF/Kevlar composite fabric showed a nonlinear distribution, and the shear-locking load was significantly higher than that of the neat fabric at the three loading rates. At the loading rate at which STF shear thickening behavior occurs (1000 mm/min), the composite fabric has the highest shear-locking load, whereas at the loading rate at which STF shear thinning occurs (500 mm/min), the shear-locking load is relatively low. Due to the effect of STF on the interfacial friction behavior of the fabric, the shear strain of the STF/Kevlar composite fabric in the shear-locking state is slightly larger than that of the neat fabric. The shear stress-strain relationship curves of neat and STF/Kevlar composite fabrics are all linear, and the shear moduli of the composite fabric is significantly higher than that of the neat fabric, due to the loading rate. At the rate of shear thickening of STF, the composite fabric has the highest shear modulus and energy absorption during shear deformation, while the shear modulus and energy absorption during shear deformation of the composite fabric is

Table 4
Cell spring torsion coefficient k (unit N/rad).

Specimen	100 mm/min	500 mm/min	1000 mm/min
Neat	3.98	3.97	4.22
STF/Kevlar	5.29	4.92	6.18

relatively low at the shear thinning rate of STF, but still slightly higher than that of the neat fabric. The theoretical model analyses of the weaving cells show that the torsion coefficient of the neat and STF/Kevlar composite fabrics have the same variation trend as the shear modulus at three loading rates, which can represent the shear deformation stiffness of the weaving cell to a certain extent. Before the shear-locking behavior occurs, the constitutive behavior of the fabric exhibits a linear relationship, which can be characterized by the spring torsion coefficient of the weaving cells.

CRedit authorship contribution statement

Yu Ma: Methodology, Investigation, Funding acquisition, Writing - original draft.

Xiang Hong: Experimental, Software, Validation.

Zhenkun Lei: Conceptualization, Investigation, Writing review & editing, Funding acquisition.

Ruixiang Bai: Resources, Software.

Yan Liu: Experimental, Calibration, Data curation.

Jiasheng Yang: Model, Validation.

Data availability statement

The raw/processed data required to reproduce these findings cannot be shared at this time due to legal or ethical reasons.

Declaration of competing interest

The authors declare that they have no competing financial interests or personal relationships that could have appeared to influence the work reported in this paper.

Acknowledgments

The authors thank the Postdoctoral Research Foundation of China (2020TQ0033), Natural Science Foundation of Chongqing (cstc2021jcyj-msxmX0643), National Natural Science Foundation of China (Nos. 11972106).

Appendix

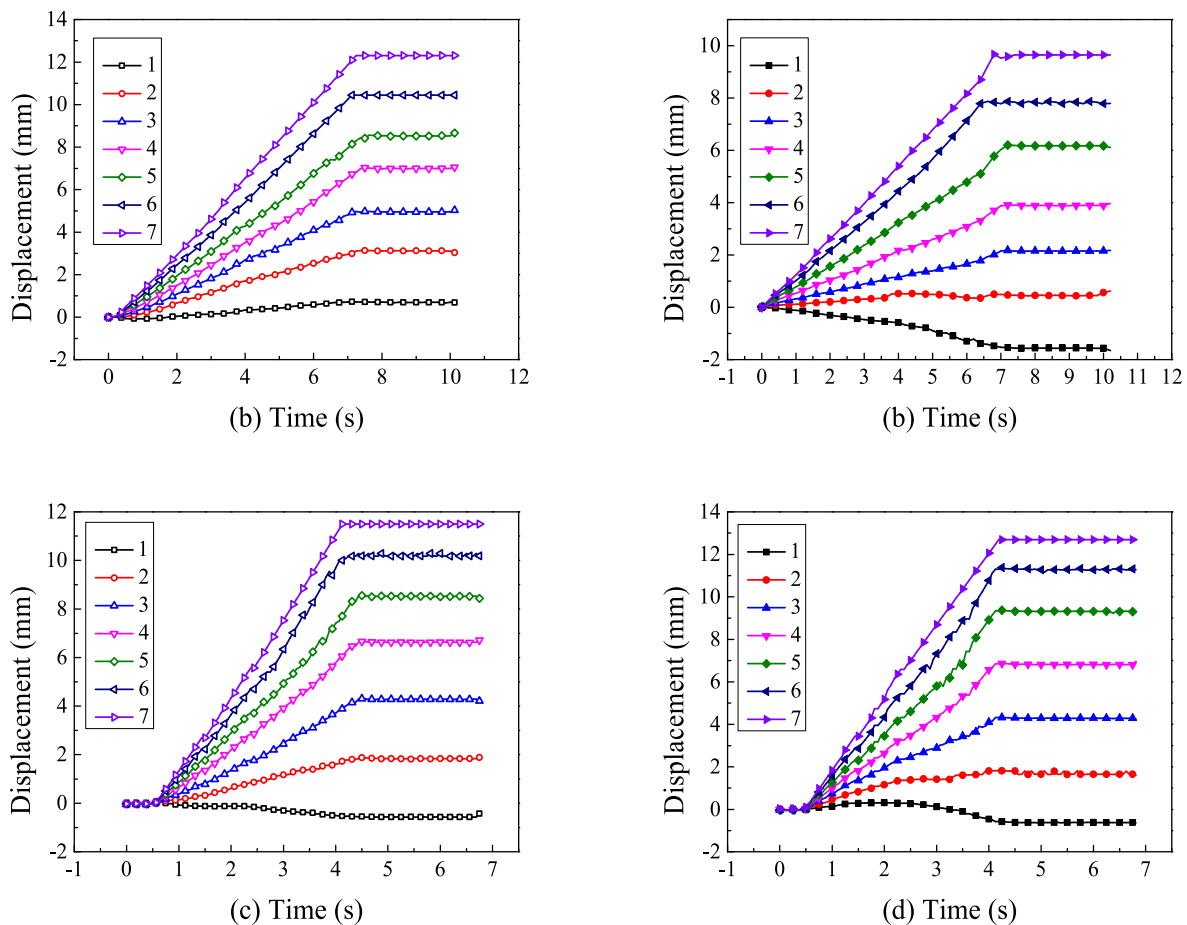


Fig. A1. Displacement in y direction of No. 1–7 markers (a) neat fabric (b) STF/Kevlar composite fabric at 500 mm/min loading rate, (c) neat fabric (d) STF/Kevlar composite fabric at 1000 mm/min loading rate

References

[1] M. Abteu, F. Boussu, P. Bruniaux, C. Loghini, I. Cristian, Ballistic impact mechanisms - a review on textiles and fibre-reinforced composites impact responses, *Compos. Struct.* 223 (2019), 110966.

[2] Sarah V. Hart, Wendy Howe, *Selection and application guide to personal body armor*, NJ Guide 100–01 (2001).
 [3] Y. Duan, M. Keefe, T. Bogetti, B. Cheeseman, Modeling friction effects on the ballistic impact behavior of a single-ply high-strength fabric, *Int. J. Impact Eng.* 31 (2005) 996–1012.

- [4] Y. Duan, M. Keefe, T. Bogetti, B. Cheeseman, B. Powers, A numerical investigation of the influence of friction on energy absorption by a high-strength fabric subjected to ballistic impact, *Int. J. Impact Eng.* 32 (2006) 1299–1312.
- [5] R. Bai, W. Li, Z. Lei, Y. Ma, F. Qin, Q. Fang, X. Chen, Y. Chen, Experimental study of yarn friction slip and fabric shear deformation in yarn pull-out test, *Compos. Appl. Sci. Manuf.* 107 (2018) 529–535.
- [6] R. Bai, Y. Ma, Z. Lei, Y. Feng, C. Liu, Energy analysis of fabric impregnated by shear thickening fluid in yarn pullout test, *Composites Part B* 174 (2019), 106901.
- [7] F. Qin, Z. Lei, Y. Ma, Q. Fang, R. Bai, W. Qiu, C. Yan, Y. Feng, Stress transfer of single yarn drawing in soft fabric studied by micro Raman spectroscopy, *Composites Part A* 112 (2018) 134–141.
- [8] Z. Lei, F. Qin, Q. Fang, et al., Full-field fabric stress mapping by micro Raman spectroscopy in a yarn push-out test, *Appl. Opt.* 57 (2018) 924–930.
- [9] R. Bai, Y. Ma, Z. Lei, Y. Feng, D. Liu, C. Yan, Impact resistance analysis of flexible fabric by 3D shape of impact basin in low-speed impact test, *Polym. Test.* 81 (2020), 106215.
- [10] Y. Ma, Z. Lei, G. Huang, R. Bai, Y. Xu, X. Hong, Energy absorption analysis of STF/Kevlar composite fabric based on 3D morphology of impact basin under low-speed impact, *Compos. Struct.* 283 (2022), 115152.
- [11] P. Harrison, F. Abdiwi, Z. Guo, et al., Characterising the shear-tension coupling and wrinkling behaviour of woven engineering fabrics, *Compos. Appl. Sci. Manuf.* 43 (2012) 903–914.
- [12] F. Nosrat, T. Gereke, C. Eberdt, et al., Characterisation of the shear-tension coupling of carbon-fibre fabric under controlled membrane tensions for precise simulative predictions of industrial preforming processes, *Compos. Appl. Sci. Manuf.* 67 (2014) 131–139.
- [13] M. Moezzia, J. Yekrang, A. Khodadad, M. Hatami, Characterizing the wrinkling behavior of woven engineering fabrics with local non-uniformity, *Composites Part A* 118 (2019) 20–29.
- [14] M. Wei, K. Lin, L. Sun, Shear thickening fluids and their applications, *Mater. Des.* 216 (2022), 110570.
- [15] A. Khodadadi, G. Liaghat, A. Taherzadeh, D. Shahgholian, Impact characteristics of soft composites using shear thickening fluid and natural rubber-A review of current status, *Compos. Struct.* 271 (2021), 114092.
- [16] S. Cao, H. Pang, C. Zhao, S. Xuan, X. Gong, The CNT/PSt-EA/Kevlar composite with excellent ballistic performance, *Composites Part B* 185 (2020), 107793.
- [17] Y. Xu, H. Zhang, G. Huang, Ballistic performance of B4C/STF/Twaron composite fabric, *Compos. Struct.* 279 (2022), 114754.
- [18] G. Nilakantan, R. Merrill, M. Keefe, J. Gillespie, E. Wetzal, Experimental investigation of the role of frictional yarn pullout and windowing on the probabilistic impact response of kevlar fabrics, *Composites Part B* 68 (2015) 215–229.
- [19] W. Na, H. Ahn, S. Han, et al., Shear behavior of a shear thickening fluid-impregnated aramid fabrics at high shear rate, *Composites Part B* 97 (2016) 162–175.
- [20] G. Lin, Z. Wan, X. Du, Two-dimensional shear models of prepreg woven fabrics, *Acta Mater. Compos. Sin.* 5 (2006) 149–153.